energies

MDPI

Article

Comparative Simulation and Optimization of "Continuous Membrane Column" Cascades for Post-Combustion CO_2 Capture

Kirill A. Smorodin [1], Artem A. Atlaskin [1,*], Sergey S. Kryuchkov [1], Maria E. Atlaskina [1], Nikita S. Tsivkovsky [1], Alexander A. Sysoev [1], Vyacheslav V. Zhmakin [1], Anton N. Petukhov [2], Sergey S. Suvorov [2], Andrey V. Vorotyntsev [2,3] and Ilya V. Vorotyntsev [1]

[1] SMART Polymeric Materials and Technologies Laboratory, Mendeleev University of Chemical Technology of Russia, 125047 Moscow, Russia
[2] Chemical Engineering Laboratory, National Research Lobachevsky State University of Nizhny Novgorod, 603022 Nizhny Novgorod, Russia
[3] Faculty of Chemistry, Lomonosov Moscow State University, 119991 Moscow, Russia
* Correspondence: atlaskin.a.a@muctr.ru

Abstract

This study presents a comprehensive evaluation of a modified membrane cascade operating in "Continuous Membrane Column" mode for selective CO_2 capture in combined heat power plants. For the first time, a novel membrane cascade configuration for separating four-component wet flue gases is analyzed and compared with existing technologies in terms of the capital and operating costs required to capture one ton of CO_2. The proposed membrane cascade generates two countercurrent recirculating streams: one continuously depleted of the permeate component and the other enriched in it. Because the internal recirculation streams significantly exceed the bypass product streams, the system demonstrates a multiplicative increase in separation efficiency. As a result, the required membrane area and compression energy can be significantly reduced. The analysis demonstrates that the proposed cascade configuration meets all current performance requirements for CO_2 recovery and the target composition of the product and residual streams. Furthermore, due to its balanced material and energy cost ratio, the system can serve as a competitive alternative to previously developed membrane CO_2 capture technologies, offering lower overall capture losses.

Keywords: flue gases; carbon dioxide; membrane; cascade; process design; simulation

Check for updates

Academic Editors: Cinthia Maia Pederneiras, Maria Margarida Mateus, José Condeço and Luisa Marques

Received: 11 December 2025
Revised: 29 December 2025
Accepted: 30 December 2025
Published: 7 January 2026

Copyright: © 2026 by the authors. Licensee MDPI, Basel, Switzerland. This article is an open access article distributed under the terms and conditions of the Creative Commons Attribution (CC BY) license.

1. Introduction

The continuous growth of carbon dioxide emissions driven by industrial expansion is widely recognized as a major contributor to global warming [1]. In response, international mitigation strategies aimed at limiting temperature rise to 1.5 °C require rapid and substantial reductions in CO_2 emissions, ultimately achieving net-zero levels by 2050 [2]. Within the framework of carbon capture and storage (CCS) technologies, three major approaches to CO_2 processing are commonly distinguished: pre-combustion technologies, involving carbon removal from fossil fuels prior to combustion [3]; oxy-combustion technologies, which rely on generating an oxygen-rich environment within the combustion unit [4]; and post-combustion technologies, aimed at capturing CO_2 from flue gases of combined heat power plants (CHPP), steelworks, cement plants, and similar facilities [5].

The first two approaches—pre-combustion and oxy-combustion—are more suitable for newly designed industrial installations. In contrast, post-combustion CO_2 capture units

can be retrofitted into existing process lines with relative ease. For this reason, significant research efforts have been dedicated either to the development of new post-combustion CO_2 capture processes [6,7] or to the optimization and intensification of established technologies [8,9].

At present, amine scrubbing remains the most widely applied post-combustion CO_2 capture technique. In this process, aqueous solutions of monoethanolamine or methyldiethanolamine chemically absorb CO_2 from flue gases [10–12]. As of 2021, 19 large-scale amine-based capture units were in operation, collectively removing more than 39 million tons of CO_2 per year [13–16]. Despite its widespread adoption, amine scrubbing is associated with substantial drawbacks: capture costs may reach up to USD 111 per ton of CO_2, largely due to the very high energy demand for solvent regeneration (>3000 MJ per ton CO_2) [17,18]. Furthermore, solvent degradation leads to the formation of numerous byproducts—including carboxylic and amino acids, aldehydes, amides, ammonia, and others generated via thermal decomposition [19] in the presence of oxygen [20,21]. Many of these products form heat-stable salts that do not decompose during desorption, thereby reducing sorbent capacity and altering its physicochemical properties, promoting foaming, corrosion, and equipment deterioration [22]. These limitations motivate the search for alternative approaches, among which membrane-based gas separation has emerged as a promising option [23,24]. Membrane technology is reagent-free, modular, requires neither heat supply nor removal, and has minimal environmental impact.

A large number of membrane-based process concepts have been proposed for CO_2 capture at CHPPs. Favre [25] compared membrane systems with conventional technologies and identified operating windows where membrane separation can compete with amine absorption. He highlighted that membrane processes relying solely on feed compression become attractive only when CO_2 concentration exceeds ~20%, due to the high CAPEX and OPEX associated with gas compression. Alternatively, vacuum operation on the permeate side can reduce compression costs but demands large membrane areas of highly permeable materials. Building on these insights, Yang et al. [26] proposed a two-stage membrane configuration with recycling, reporting capture penalties of 45–80 USD per ton CO_2. Zhao and co-authors evaluated 14 membrane process designs [27], concluding that a two-stage cascade with retentate recycle in the second stage offers the lowest energy consumption for producing CO_2 at 95% purity and 95% recovery. Merkel et al. further examined two-step vacuum and counter-flow/sweep configurations through simulation and demonstrated that capture costs may be reduced to USD 23 per ton CO_2. However, many simulation studies rely on hypothetical membranes with unrealistically high transport properties or lab-scale materials whose production costs cannot be reliably estimated [28–30].

The present study provides a comprehensive investigation of membrane-based CO_2 capture for CHPP applications. Four process configurations—including two novel designs—were analyzed through rigorous simulation. Particular focus was placed on evaluating two membrane cascade concepts of the "Continuous Membrane Column" type and comparing them with two-step vacuum and two-step counter-flow/sweep schemes. The analysis considered separation of a four-component wet flue gas mixture produced by a 600 MW CHPP. Key performance criteria included CO_2 recovery ($\geq$90%), CO_2 purity in the product stream ($\geq$95 mol.%), and residual CO_2 concentration in the vent gas ($\leq$2 mol.%). Sensitivity analysis was used to optimize membrane area requirements for all configurations, followed by a techno-economic comparison. Based on these results, the most promising process design was identified and recommended for industrial implementation.

2. Single-Membrane Unit Model

The simulation of the integrated process for capturing carbon dioxide from flue gas was constructed using individual membrane modules interconnected with each other and with auxiliary process units. Each membrane module can operate either in a conventional counter-current configuration or in a sweep-assisted mode, in which the permeate stream is diluted by an external sweep gas. The overall separation process was simulated in Aspen Plus v. 9.0 (Bedford, MA, USA), into which a custom membrane-module block developed in Aspen Custom Modeler was incorporated. This block represents a hollow-fiber membrane module originally designed by Ajayi and Bhattacharyya within the U.S. Department of Energy's Carbon Capture Simulation Initiative (CCSI) [31].

This study employs a one-dimensional, multicomponent membrane model formulated as a system of partial differential equations (PDEs) describing mass transfer. This model is applicable to membrane materials governed by the solution–diffusion mechanism, where component permeances remain independent of pressure, concentration, and stage cut, and the overall separation process is treated as isothermal. A notable feature of the model is its capability to compute pressure drops along both the lumen (bore) and shell sides of the hollow fibers using the Hagen–Poiseuille equation for compressible fluids.

In the simulated configuration, feed gas enters on the shell side of the membrane fibers and permeates into the bore side. The permeate can be withdrawn directly or swept with an auxiliary stream (e.g., air or nitrogen). The module is assumed to operate at a steady state, with counter-current flow established between the feed and permeate sides. The gas mixture is treated as ideal, and the model generates axial profiles of concentration gradients and component fluxes. Owing to its equation-oriented formulation, the model offers high flexibility, enabling both rating and design calculations by specifying appropriate degrees of freedom.

Geometric parameters of the hollow fibers, together with mass flow constraints, are summarized in Table 1, and the process flow diagram is presented in Figure 1.

Table 1. Detailed information on membrane unit module.

Variable	Typical	Base Case
Inner Fiber Diameter, μm	100–700	400
Outer Fiber Diameter, μm	200–800	600
Effective Fiber Length, m	0.15–1.50	1.00
Permeance, GPU *	10–10,000	1000

* 1 GPU = 1×10^{-6} cm^3 (STP) cm^{-2} s^{-1} $cmHg^{-1}$.

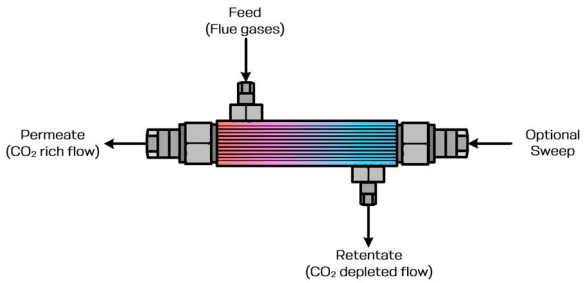


Figure 1. Flow diagram of the membrane unit model.

3. Designs of the Technological Schemes

To identify the optimal membrane-based process configuration for CO_2 capture from CHPP flue gas, four alternative designs were evaluated using Aspen Plus simulations under identical input conditions. In addition to defining the properties of the feed stream,

it is essential to establish membrane permeance (Q, GPU) and selectivity (α) values that will be used consistently across all tested configurations. For sensitivity analysis, all other parameters, such as membrane permeance, membrane area, and feed and permeate pressures, should remain fixed.

The present study examines process performance under conditions close to industrial operation. Specifically, it considers a four-component flue gas mixture generated by a 600 MW combined heat and power plant (CHPP), as analyzed in [32]. In addition, this study compares two modified membrane cascade configurations incorporating an integrated condenser with the process schemes proposed by Merkel et al. [32], which represent the only industrially tested membrane-based CCS implementation to date [33]. Four designs were therefore evaluated in the Aspen Plus environment: two original cascade configurations of "Continuous Membrane Column" type (Figure 2) and two designs proposed by Merkel et al. [32]—namely, the two-step vacuum process and the two-step counter-flow/sweep process.

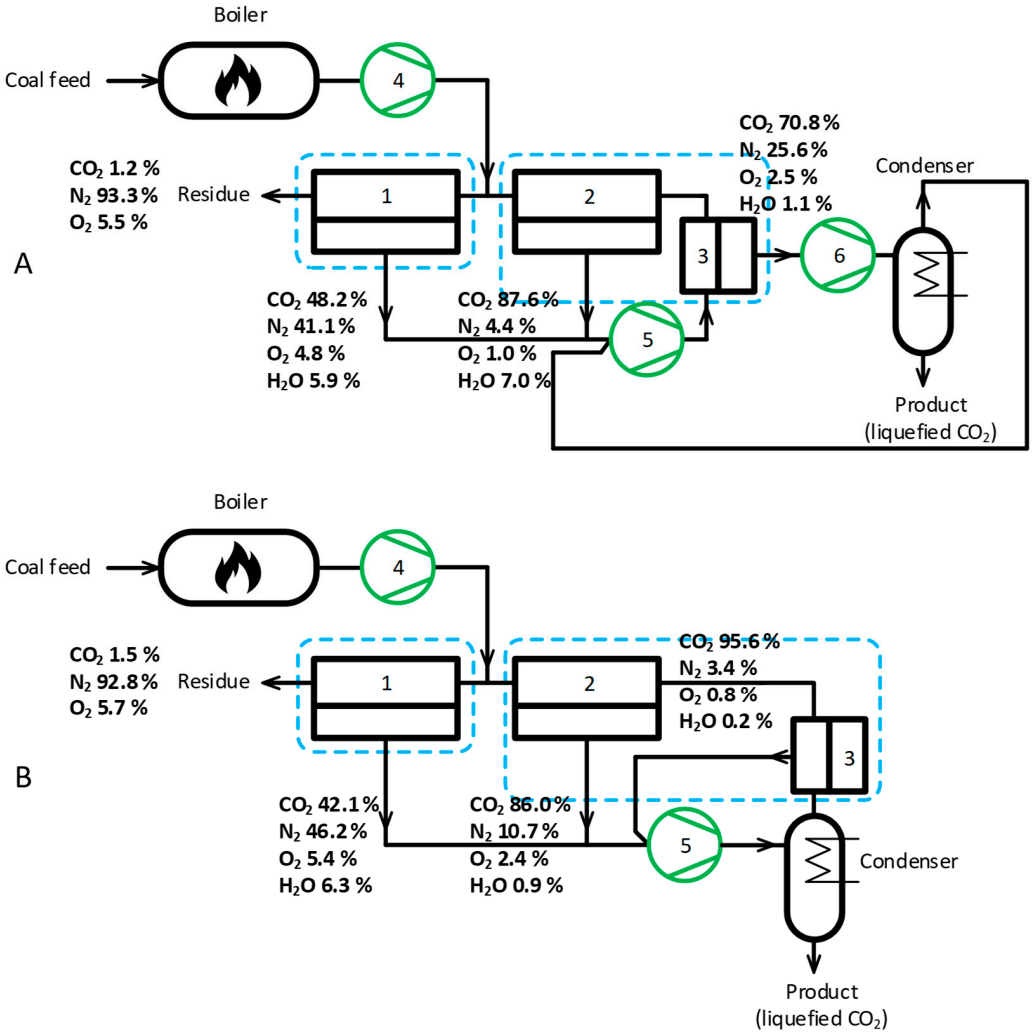


Figure 2. Principal schemes of membrane cascade type of "Continuous membrane column" modified with condenser: (**A**) condenser on the permeate side of enrichment section; (**B**) condenser on the recycled permeate side of enrichment section. 1, 2, 3—membrane modules; 4, 5, 6—compressors.

Unlike conventional multi-stage or multi-step cascades, where separation efficiency is increased by recycling large retentate or permeate streams between discrete stages—thereby increasing compression duty, membrane area, and process complexity—the proposed configuration type of "Continuous Membrane Column" [34,35] relies on internally coupled

countercurrent recirculation within a single cascade framework. This internal circulation creates two continuously interacting streams: one progressively depleted of and the other progressively enriched in CO_2, resulting in a multiplicative enhancement of separation efficiency rather than an additive stage-by-stage effect.

A key advantage is that the internal recirculating flows significantly exceed the net product flows, which allows the target CO_2 recovery and purity to be achieved with a substantially lower total membrane area. In particular, it is expected that in comparison with conventional cascades with recycling, the proposed design reduces total membrane area or vacuum-compressor units' energy consumption.

All systems were simulated under identical operating conditions and using consistent compressor and condenser characteristics. The feed to all separation schemes was wet flue gas containing CO_2, N_2, O_2, and water vapor.

Both original cascade designs operate according to the same general principle. After the boiler, the flue gas is introduced at an intermediate point between membrane stages (1) and (2). Conceptually, the cascade can be divided into a stripping section and an enrichment section, each serving distinct separation objectives. The stripping section comprises the pack of membrane modules (1), where a CO_2-depleted retentate stream is produced, while the CO_2-rich permeate is directed toward compression. The enrichment section comprises stages (2) and (3), where the permeate is further concentrated in CO_2. The principal difference between the two proposed schemes lies in the operation of the final membrane stage (3).

In the configuration (Figure 2A), the permeate streams from modules 1 and 2 are combined upstream of compressor 5 and then fed into membrane module 3. The CO_2-rich permeate from module 3 flows to the condenser, where liquid CO_2 is recovered. The non-condensed, CO_2-lean fraction is subsequently routed to compressor 5. In the configuration (Figure 2B), compressor 5 receives the permeate streams from all membrane modules simultaneously and delivers the combined stream directly to the condenser, where liquid CO_2 is obtained. The water is removed sequentially on each compressor unit. In this way, for cascades in Figure 2A,B and two-step counter-flow/sweep processes, the water content reduces in following manner: after the first compression stage, it reduces from 11 to 2.1 mol.%, and then before the condenser it is reduced up to 1.1 mol.%. In the two-step vacuum design, due to the recirculation flow from the permeate side of the second step, the water content does not reduced as efficiently as in previous cases, and this happens as follows: first, compression allows the water content to reduce to 9.4 mol.%, and prior to condensation it reduces to 4.7 mol.%.

The key performance requirements for all investigated processes are as follows:

- CO_2 recovery $\geq$ 90%,
- Product stream purity $\geq$ 95 mol.%,
- CO_2 concentration in the vent gas $\leq$ 2 mol.%.

Achieving these targets is complicated by the inherently low CO_2 partial pressure in flue gas, which arises from both low CO_2 concentration and the near-ambient total pressure of the stream. Consequently, establishing sufficient transmembrane driving force requires increasing the feed-side pressure, reducing the permeate-side pressure, or applying a combination of both approaches. Identifying the optimal balance between feed compression and permeate pumping is therefore essential for minimizing energy consumption while respecting practical operating constraints.

For instance, Micari et al. [28] investigated permeate-side pressures ranging from 0.01 to 0.10 bar. However, such deep vacuum levels are rarely attainable in large-scale industrial pumping systems. In practice, a residual pressure of 0.15–0.20 bar is often considered the lowest feasible limit for flue gas CO_2 capture, and in some specific cases,

0.1 bar is reached [36]. Operation below this range leads to disproportionately large pump dimensions, increased manufacturing precision requirements, and sharply elevated equipment costs. Furthermore, even if such pressures could be applied, the actual permeate pressure within the membrane module would be higher due to pressure drop along the fiber channels. Achieving pressures in the 0.01–0.10 bar range also imposes stringent constraints on valves, fittings, and auxiliary equipment, all of which must meet exceptionally low leakage standards.

The full set of input parameters used in the simulations is provided in Table 2. Due to the lack of data on the specific case for which the mass transfer characteristics of the membrane were measured, it is assumed that they are constant for all stages of the membrane cascade.

Table 2. Input data of the feed flow.

Parameter	Value
Feed flow, kmol h^{-1}	67,543.8
Pressure, MPa	0.1
Temperature, °C	50
Composition, mol.%	
N_2	73
CO_2	11.6
H_2O	11
O_2	4.4

4. Results and Discussion

The first step is to determine an appropriate membrane permeance range based on the current state of membrane technology and its readiness for large-scale deployment, meaning the ability to manufacture millions of square meters of hollow-fiber membranes or, at minimum, thin-film materials suitable for spiral-wound modules. According to the 2008 Robeson plot [37], the updated Robeson upper bound by Zhang et al. [38,39], and the permeability data summarized by Min Liu et al. [40], commercially relevant CO_2 permeance values typically fall within the range of 700–5500 GPU. Extremely high permeance values—up to 20,000 GPU—have been reported for poly(1-trimethylsilyl-1-propyne) (PTMSP) thin films; however, their CO_2/N_2 selectivity is modest (~3.6), and PTMSP suffers from significant physical aging due to free-volume collapse, leading to rapid deterioration of gas-transport properties.

He et al. [30] reported laboratory-scale graphene-based membranes with permeance up to 11,790 GPU and selectivity up to 57.2. Nevertheless, as Micari et al. [28] emphasized, such membranes can currently be produced only as 10 × 50 cm films, making them unsuitable for industrial-scale application. By contrast, Merkel of MTR (Membrane Technology and Research) [41] reported in 2022 that Polaris membrane generations 1–3 exhibit CO_2 permeance values between 1000 and 3000 GPU. The first generation has already undergone pilot-scale testing for CO_2 capture, while the second and third generations are still in laboratory evaluation.

Based on the available data, it can be concluded that, at present, the only commercially viable membrane type combining scalability and established performance offers CO_2 permeance around 1000 GPU. The corresponding selectivity of approximately 50 may exceed the practical requirements of the targeted separation task; therefore, its optimal value will be determined through further simulation.

4.1. Effect of Membrane Selectivity

The simulation-based analysis was conducted for both original membrane cascade configurations presented in Figure 2. In the base case, the membrane permeance was set to 1000 GPU, while the membrane area was fixed at 5.13×10^6 m^2 for the stripping section and 3.12×10^5 m^2 for the enrichment section. The influence of CO_2/N_2 selectivity was evaluated according to two key performance criteria: the CO_2 concentration in the product stream (obtained from the enrichment section) and the CO_2 concentration in the residue stream (withdrawn from the stripping section). The resulting trends are presented in Figure 3.

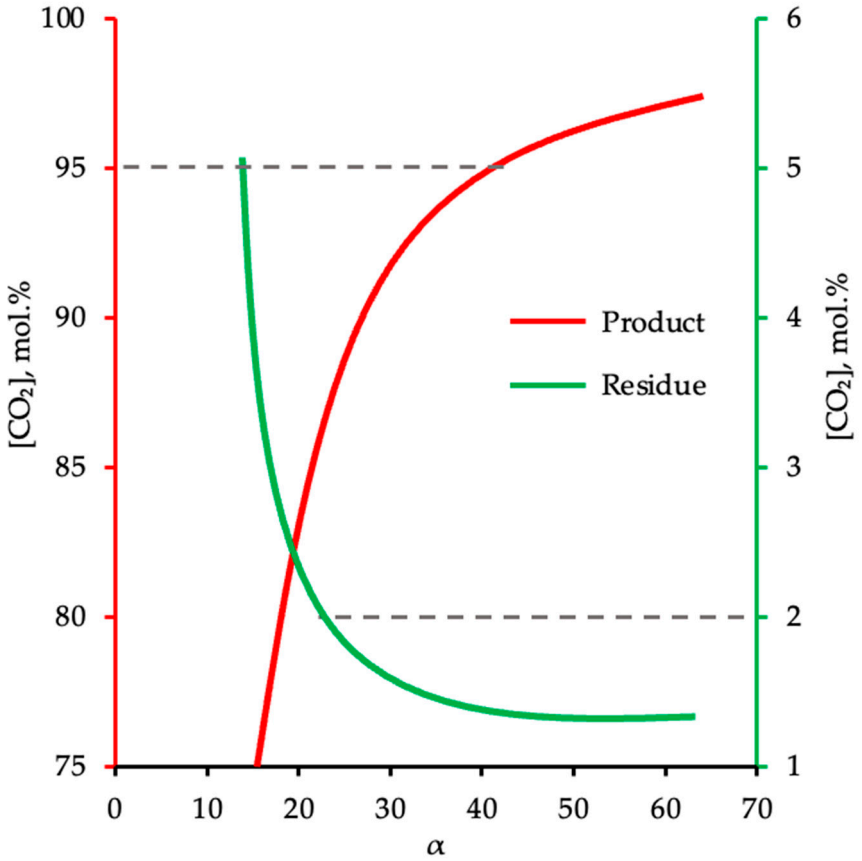


Figure 3. The dependence of carbon dioxide content in product (left red axis) and residue (right green axis) streams on membrane selectivity value at a constant membrane permeance and area. Dotted lines illustrate the target value of CO_2 content level.

As illustrated by the simulation results in Figure 3, membrane selectivity has a pronounced impact on the ability of the process to meet the target CO_2 concentrations in both the product and residue streams. Membranes with a CO_2/N_2 selectivity of 20–21 or lower cannot reduce the CO_2 content in the residue stream to below 2 mol.%. Conversely, achieving a product stream with a CO_2 concentration of at least 95 mol.% requires a minimum membrane selectivity of approximately 48.

The observed dependence is attributed to the need for rapid enrichment of the permeate stream in CO_2 within the stripping section, followed by further concentration in the enrichment section. Because the flue gas contains CO_2 at a very low partial pressure, high selectivity is essential to generate a sufficiently enriched permeate after the first membrane stage. When membrane selectivity is inadequate, the feed to the enrichment section remains insufficiently enriched, making it impossible to reach the required product purity of 95 mol.% or higher.

Therefore, even a substantial increase in membrane area cannot compensate for low selectivity, and no process optimization strategy or redesign of the separation scheme can overcome the fundamental limitations imposed by membranes with insufficient mass-transfer performance.

4.2. Effect of Membrane Area

Once the mass-transfer characteristics of the membrane were established, the next step was to evaluate how the membrane area in the stripping and enrichment sections affects the ability of the process to meet its separation targets and to determine the minimum membrane area—hence, capital cost—required in each section of the cascade. To study the influence of membrane area, the following approach was adopted. For example, when assessing the effect of membrane area in the enrichment section, the fixed membrane area was first assigned to the stripping section, while the enrichment-section area was varied over a specified range. This procedure was repeated for multiple fixed values of the stripping-section membrane area. As a result, a set of data points describing the dependence of process performance on the enrichment-section membrane area was obtained for each chosen value of the stripping-section area, enabling the construction of continuous curves. An identical procedure was performed to examine the influence of the stripping-section membrane area.

Because the internal mass flows of the cascade form a closed loop, any change in membrane parameters in one section affects the operating conditions of the entire system. Consequently, it is not feasible to study the effect of each section independently. The only appropriate methodology is to evaluate both sections simultaneously—a consideration that applies to all configurations examined in this study.

Figure 4 illustrates the dependence of CO_2 recovery on the membrane area in the enrichment section for various fixed membrane areas in the stripping section for the cascade shown in Figure 2A. The enrichment-section membrane area varied from 2.6×10^5 to 4.1×10^5 m^2. The results indicate that CO_2 recovery rates exceeding 90% can be achieved only when the enrichment section membrane area reaches at least 3.3×10^5 m^2. However, achieving this minimum enrichment-section area requires a membrane area of 5.2×10^6 m^2 in the stripping section.

A moderate increase in total membrane area—raising the enrichment-section area to 3.8×10^5 m^2—significantly reduces the required stripping-section area to 3.3×10^6 m^2, yielding a savings of 1.9×10^6 m^2. This effect results from two simultaneous phenomena: (i) increased permeation of CO_2 through the membranes, and (ii) a corresponding reduction in the amount of CO_2 circulating within the cascade. Together, these factors eliminate the need to further increase the membrane area in the stripping section.

Next, the influence of the membrane area in the stripping section on CO_2 recovery was examined at several fixed membrane areas in the enrichment section. Figure 5 presents the resulting dependencies. As the graphs demonstrate, variations in the stripping-section membrane area at four constant enrichment section areas have a pronounced effect on the recovery rate.

Membrane areas in the stripping section of 3.0×10^6 m^2 or below do not allow the process to achieve the required CO_2 recovery. In contrast, a stripping section membrane area of 3.15×10^6 m^2, combined with 4.3×10^5 m^2 of membrane in the enrichment section, meets the target recovery of 90%, and this combination yields the minimum total membrane area—3.53×10^6 m^2.

As noted previously, even a modest increase in membrane area within the enrichment section leads to substantial reductions in the membrane area required in the stripping section—up to 7.3×10^5 m^2, which corresponds to nearly 170% of the total enrichment-

section area. For comparison, if the process operates with 3.3×10^5 m^2 of membrane in the enrichment section, the stripping section must contain approximately 6.0×10^6 m^2 of membrane to achieve the same performance.

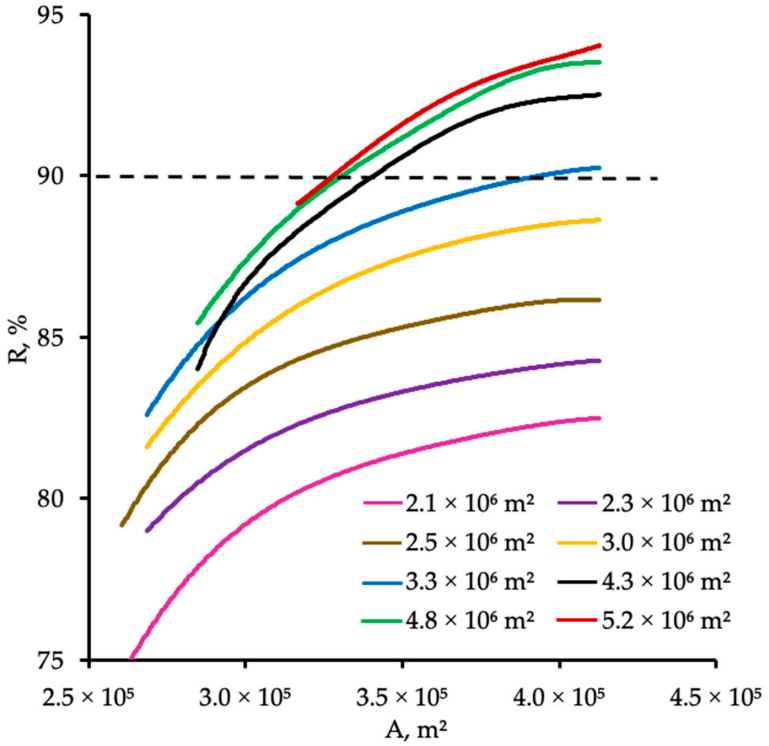


Figure 4. Influence of the membrane area (A) on the carbon dioxide recovery rate (R) in the enrichment section at eight different and constant membrane areas in the stripping section. Dotted lines illustrate the target value of CO_2 recovery rate.

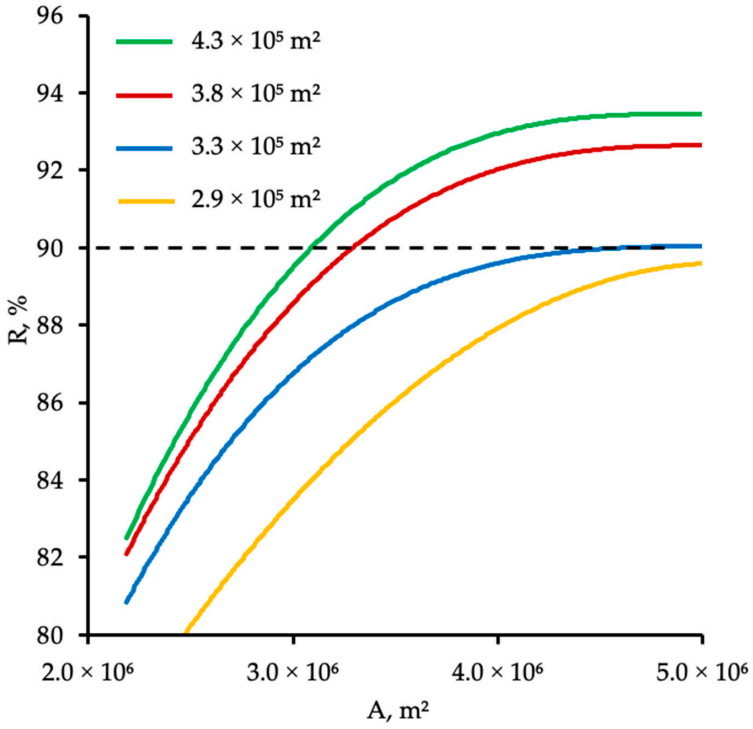


Figure 5. Influence of the membrane area (A) on the carbon dioxide recovery rate (R) in the stripping section at four different and constant membrane areas in the enrichment section. Dotted lines illustrate the target value of CO_2 recovery rate.

When considering the second key objective of the process—achieving a CO_2 purity of 95 mol.% in the product stream—it is important to note that meeting the recovery-rate requirement simultaneously ensures the desired product composition across the entire investigated range of membrane areas. Figure 6 illustrates the effect of the enrichment-section membrane area on CO_2 purity in the product stream for several fixed values of the membrane area in the stripping section. As the graphs show, all examined membrane-area combinations yield product streams with CO_2 concentrations above 95 mol.%. Even at relatively small membrane areas—2.1×10^6 m^2 in the stripping section and approximately 2.6×10^5 m^2 in the enrichment section—the target purity is achieved. Moreover, at the lowest membrane-area values tested in both sections, the process produces a product stream containing more than 99 mol.% CO_2.

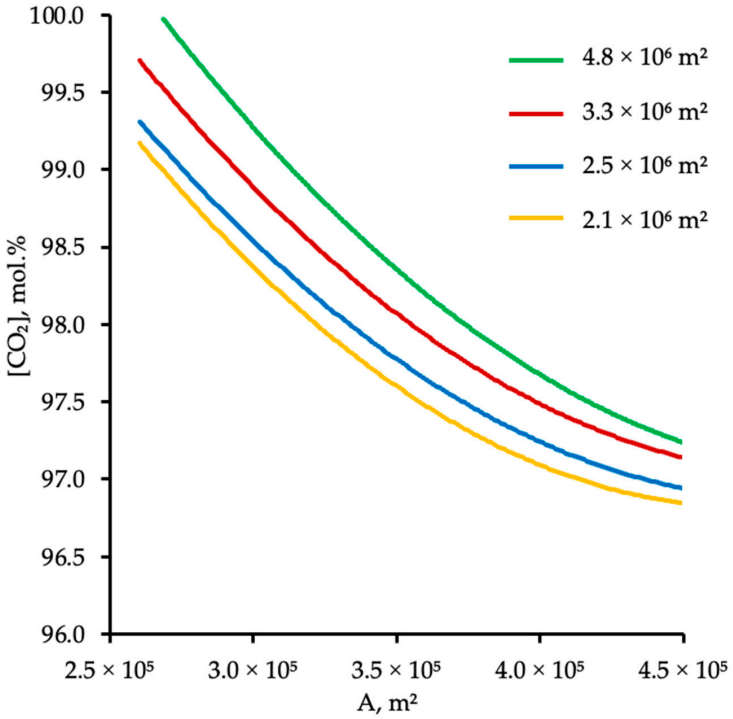


Figure 6. Influence of the membrane area (A) on the carbon dioxide concentration in the product stream in the enrichment section at four different and constant membrane areas in the stripping section.

Figure 7 presents the influence of membrane area in the stripping section on the CO_2 concentration in the residual stream. Within the examined range, stripping-section membrane areas of 2.5×10^6 m^2 or greater ensure that the CO_2 content in the vent gas does not exceed the required limit.

Overall, the results demonstrate that the proposed configuration—a membrane cascade of the "Continuous Membrane Column" type—readily achieves the product-purity target of $\geq$95 mol.% CO_2. Thus, the principal challenge for this process lies not in meeting the purity specification but in attaining the required CO_2 recovery rate.

In addition, three further membrane-based process configurations were optimized with respect to their required membrane areas, followed by a techno-economic assessment comparing the CO_2 capture penalty (CAPEX and OPEX) for all evaluated designs. For the membrane cascade shown in Figure 2B, the minimum total membrane area needed to achieve CO_2 recovery above 90% and product purity exceeding 95 mol.% is 2.8×10^6 m^2.

The substantial reduction in membrane area relative to the configuration in Figure 2A is attributed to differences in flow organization between the enrichment-section modules and the condenser. In the configuration of Figure 2B, most of the CO_2 entering the enrichment

section is removed during condensation, thereby reducing the load on the downstream membrane stage. Consequently, only about 14,000 m^2 of membrane area is required to capture the remaining fraction of CO_2 that is not separated in the condenser, eliminating the need for large membrane modules for the final concentration.

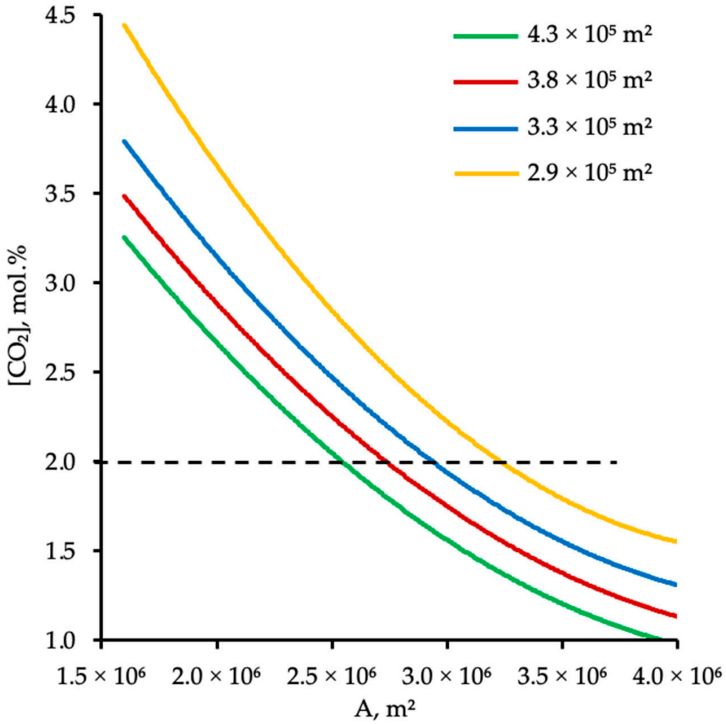


Figure 7. Influence of the membrane area (A) on the carbon dioxide concentration in the residual stream in the stripping section at four different and constant membrane areas in the enrichment section. Dotted lines illustrate the target value of CO_2 content level.

4.3. Feasibility Study for Carbon Dioxide Capture from CHPP Flue Gases

The main technological parameters of the process were determined based on the correlation analysis presented above (Table 3).

The following formula [32] was used to calculate the cost of CO_2 extraction per ton:

$$C_c = \frac{(P \times T \times E) + (0.2 \times C)}{F_{CO_2} \times T}, \quad (1)$$

where C_c is the capture cost per ton of CO_2, USD/ton CO_2; P is the electrical power required for compressor machinery operation, kW; T is the CHPP capacity factor (operating time per year), h/year; E is the electricity cost, USD/kWh; C is the capital cost of hardware, USD; and F_{CO_2} is the mass flow of captured CO_2, ton/h.

The capital costs of the equipment can be calculated from the following simplified formula:

$$C = (A_1 + A_2 + A_3) \times S_M + S_C, \quad (2)$$

where A_i are the area of membrane used, m^2; S_M is the cost of 1 m^2 of membrane, USD/m^2 (USD ~50/m^2 based on the MTR Polaris™ (New Ark, NJ, USA) membrane manufacturer [32]); and S_C is the cost of compressor units, USD.

The compression power requirements were calculated according to the following formula:

$$P = P_{C1} + P_{C2} + P_{C3}, \quad (3)$$

where P_{C1}, P_{C2}, and P_{C3} are the power consumption of compressors C1, C2, and C3, respectively, if applicable. P_{C1}, P_{C2}, and P_{C3} are each calculated via the following formula:

$$P_{Ci} = L_{in} \times \frac{\gamma}{(\gamma - 1)} \times \frac{RT_{in}}{n_v} \times \left[\left(\frac{P_{out}}{P_{in}} \right)^{\frac{\gamma-1}{\gamma}} - 1 \right] \Big/ 1000, \quad (4)$$

where P_{Ci} is power consumption, kW; L_{in} is compressor inlet flow, mol/s; γ is adiabatic expansion coefficient of the gas mixture; R is the universal gas constant; T_{in} is inlet gas temperature, K; n_v is compressor efficiency; and P_{out} and P_{in} are compressor inlet and outlet pressures, respectively.

Table 3. Key process parameters of the CO_2 processing in the membrane cascade during its capture from CHPP flue gases.

Parameter	Value	Units
Pressure in the feed side, MPa	0.15	MPa
Pressure in the permeate side, MPa	0.02	MPa
Membrane area, m^2		
Membrane permeance, GPU	1000	GPU
α (CO_2/N_2)	50	
α (CO_2/H_2O)	0.3	
α (CO_2/O_2)	12.5	
CO_2 content, mol.%		
Product flow	$\geq$95	mol.%
Residual flow	$\leq$2	mol.%
Cascade A (Figure 2A)		
Stripping section	3.15×10^6	m^2
Enrichment section	4.3×10^5	m^2
Cascade B (Figure 2B)		
Stripping section	2.8×10^6	m^2
Enrichment section	1.4×10^4	m^2
Merkel et al. [32]		
Two-step vacuum design		
Step 1	1.7×10^6	m^2
Step 2	2.5×10^6	m^2
Merkel et al. [32]		
Two-step counter-flow/sweep design		
Step 1	3.5×10^6	m^2
Step 2	2.6×10^5	m^2

The adiabatic expansion coefficient of the gas mixture was acquired from the Aspen™ Properties database.

The efficiency of operation varies for vacuum and compression pumps. To incorporate such a factor, a formula was applied that relates the compression efficiency to the ratio of pressures at the inlet and outlet of the equipment [42]:

$$n_v = 0.1058 \times \ln\left(\frac{P_{in}}{P_{out}} \right) + 0.8746. \quad (5)$$

The calculated compression work revealed that the membrane cascades of the "Continuous Membrane Column" type shown in Figure 2A,B require a total of 136.5 MW and 130.7 MW, respectively. In comparison, the two-step vacuum design and the two-step counter-flow/sweep configuration require 285.3 MW and 117.1 MW, respectively.

Because the cost of compressor equipment with a capacity of approximately 100 $m^3 \cdot min^{-1}$ spans a wide range, its capital cost was estimated by correlating compressor power with investment cost, assuming USD 500 per kW of installed capacity. The resulting CAPEX estimates for each compressor unit are summarized in Table 4.

Table 4. Compressor unit costs for each configuration.

Compressor Unit	Costs, M USD
Cascade A (Figure 2A)	
Feed stream compressor	12.4
Vacuum-compressor unit	35.3
Pre-condenser stream compressor	20.6
Cascade B (Figure 2B)	
Feed stream compressor	12.4
Pre-condenser stream compressor	53.0
Merkel et al. [32] Two-step vacuum design	
Feed stream and recycle compressor	89.1
Pre-condenser stream compressor	53.5
Merkel et al. [32] Two-step counter-flow/sweep design	
Feed stream compressor	12.4
Pre-condenser stream compressor	46.2

The condenser unit, which operates under identical conditions for all four membrane-based process configurations, was excluded from both CAPEX and OPEX calculations. This decision reflects not only the identical nature of the condenser across all schemes but also the fact that similar condensation units are employed in a variety of CO_2 capture approaches, including amine scrubbing. Consequently, it is standard practice to evaluate and compare separation processes based solely on their core physico-chemical mechanisms and not on auxiliary units common to multiple technologies. Nevertheless, the condenser operating conditions used in this study are provided here for completeness: an operating pressure of 2.5 MPa (achieved by the upstream compressor) and an operating temperature of 239.35 K. All considered configurations were configured such that the condenser receives streams containing 70.0 $\pm$ 1.5 mol.% carbon dioxide at a total molar flow rate of approximately 10,000 $\pm$ 10% kmol/h.

Using a membrane cost of USD 50 per square meter (including housing) [32], the capital expenditures for the proposed membrane cascades (Figure 2A,B), the two-step vacuum design, and the two-step counter-flow/sweep design were estimated as USD 247.3 million, 206.1 million, 351.3 million, and 247.7 million, respectively. Assuming a CHPP capacity factor of 7446 $h \cdot year^{-1}$ and an electricity price of USD 0.04 per kWh, the corresponding CO_2 capture costs amount to USD 38.26, 34.04, 65.91, and 35.84 per ton of CO_2 for the same sequence of configurations. These results clearly indicate that the "Continuous Membrane Column" cascade with a condenser processing the combined permeate streams (Cascade B) provides the lowest CO_2 capture penalty.

The cost reduction of USD 4.22 per ton for Cascade B compared to Cascade A is primarily attributable to two factors:

A substantial decrease in the total membrane area required to achieve the same separation performance;

Lower energy consumption for gas compression.

The first factor arises from the specific internal flow arrangement in Cascade B, where permeate streams from all three membrane stages are pooled and directed to a condenser. Since the condenser removes the majority of CO_2, the membrane area required in the enrichment section is minimal. The feed to membrane stage 3 is the condenser off-gas, which is already strongly depleted in CO_2; therefore, only a small membrane area ($\approx 1.4 \times 10^4$ m^2) is needed for final polishing. In contrast, the Cascade A configuration directs only the permeate of membrane stage 3 to the condenser. As a result, a significantly larger membrane area is required to produce a CO_2-rich stream suitable for liquefaction.

Consequently, Cascade A requires membrane areas of 3.15×10^6 m^2 and 4.3×10^5 m^2 in the stripping and enrichment sections, respectively, whereas Cascade B requires only 2.8×10^6 m^2 and 1.4×10^4 m^2. The total difference of 7.66×10^5 m^2 translates into substantial capital savings. Combined with the reduced compressor capacity requirements of Cascade B, the total capital cost decreases by USD 41.19 million, and energy consumption is reduced by 5.8 MWh. In terms of footprint and volume of a membrane gas separation plant, which requires 2.8×10^6 m^2 of membrane, it may be evaluated by taking into account the packing density, which theoretically is up to 10,000 m^2/m^3 and is practically up to 8000 m^2/m^3. In this way, 2.8×10^6 m^2 of membrane requires less than 400 m^3 including shells and piping. The proposed "Continuous Membrane Column" cascades may face operation- and scale-related limitations, primarily associated with increased internal recirculation flowrates, tighter coupling between membrane sections, and higher sensitivity to pressure-drop management compared to conventional multi-stage cascades with recycle streams. On a large scale, this implies stricter requirements on module hydraulic design, control strategies, and compressor reliability to ensure stable operation. Nevertheless, it is expected that unlike traditional cascades, these limitations are partially offset by the reduced total membrane area and lower compression energy demand, which mitigate scale-up penalties and make the proposed designs competitive within the investigated operating window.

Additionally, the contributions of three major components—operational costs, membrane capital costs, and compressor capital costs—to the total CO_2 capture cost were analyzed for all configurations. The results are presented in Figure 8.

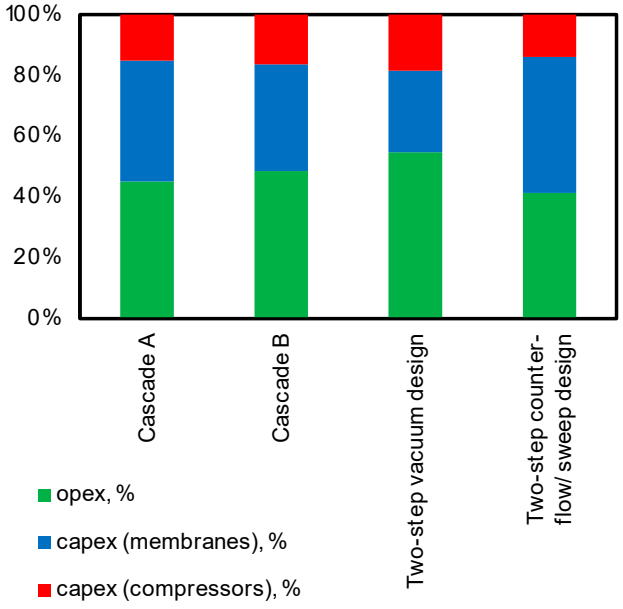


Figure 8. The impact of compressor equipment, membrane modules, and operational costs on the total CO_2 capture penalty.

As shown in the diagram, the two-step vacuum design exhibits the highest operating expenditures (OPEX), which account for nearly 55% of its total CO_2 capture cost. This makes it the least efficient configuration among those evaluated, despite having the lowest capital expenditures (CAPEX). From an investment-only perspective, such a configuration could therefore be mistakenly viewed as the most attractive option.

The two-step counter-flow/sweep design, by contrast, has the highest CAPEX among all configurations, although its OPEX represent only 41% of the total capture cost. The most balanced performance is observed for membrane Cascade B, in which CAPEX and OPEX contribute 51% and 49% of total costs, respectively.

It is also important to consider the share of membrane costs within total CAPEX, since membrane longevity directly determines future replacement investments. Among the two original cascades and the two-step counter-flow/sweep scheme, Cascade B requires the smallest membrane area. This, combined with its more favorable distribution of capital and operating costs, makes it the most suitable candidate for implementation in CHPP CO_2 capture applications.

Additionally, sensitivity analysis was performed to evaluate the impact of membrane and energy costs on the overall carbon dioxide capture penalty for all membrane plants under consideration. As is seen from the graphs in Figure 9, all dependencies are linear. It should be noted that, as it was discussed above, the two-step counter-flow/sweep design CO_2 capture costs are mostly depends on the CAPEX, and the increase in membrane costs lead to most rapid cost rise; meanwhile, another three configurations are characterized with almost the same cost increase intensity. At the same time, the analysis of energy cost impact highlights the two-step design as the most dependent configuration on this criterion. However, a comprehensive analysis of these relationships reveals that a 5-fold increase in membrane cost leads, at most, to a 2-fold increase in process costs. At the same time, a similar increase in electricity costs leads to a minimum 2.65-fold increase in process costs. Thus, all of the configurations considered are particularly sensitive to rising electricity prices. Moreover, it is possible to evaluate the capture cost ranges in the case of membrane and energy cost increase. Assuming the possible rise up to 20% on both key factors, the capture costs for considered membrane plants are 41.30, 36.43, 69.46, and 39.05 for the proposed membrane cascades (Figure 2A,B), the two-step vacuum design, and the two-step counter-flow/sweep design, respectively.

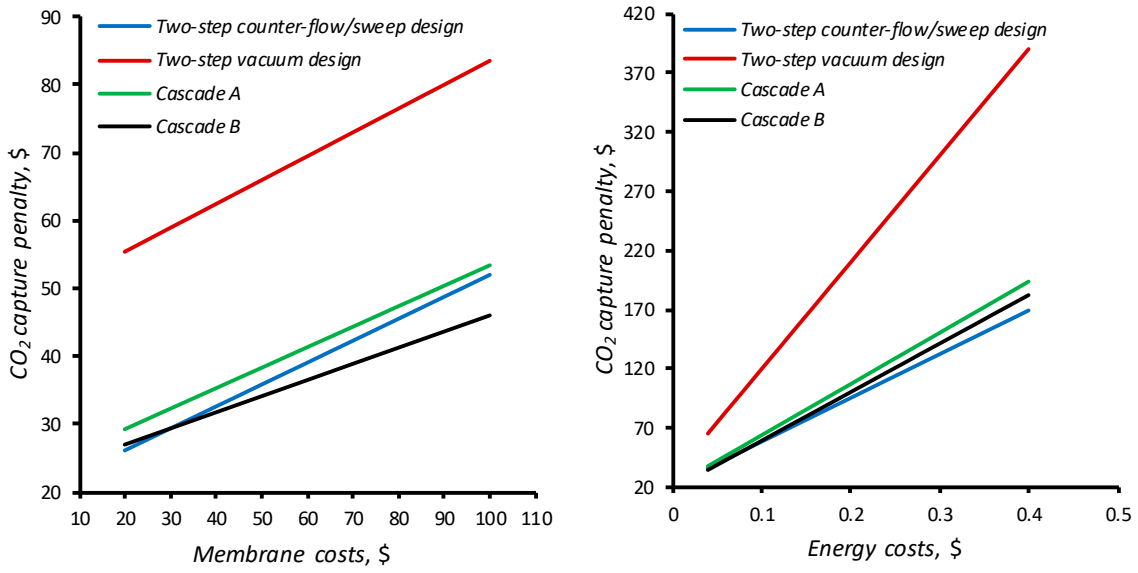


Figure 9. The impact of membrane costs ($) (**left**) and energy costs ($) (**right**) on the overall CO_2 capture penalty ($).

5. Conclusions

This study demonstrates, based on a comprehensive simulation framework and sensitivity analysis, that membrane cascades of the "Continuous Membrane Column" type can potentially enable efficient CO_2 capture from CHPP flue gas with reduced membrane area and competitive capture costs. Among the investigated configurations, Cascade A, integrating a condenser that processes the combined permeate streams, exhibited the lowest simulated CO_2 capture penalty (USD 34.04 per ton), outperforming earlier proposed two-step vacuum and counter-flow/sweep designs under the adopted assumptions. At the same time, the presented results should be interpreted in light of several modeling limitations. In particular, uncertainties remain regarding the accurate determination of membrane mass-transfer characteristics in humid multicomponent gas mixtures, as well as the extrapolation of membrane performance and pressure-drop behavior to the scaled-up multi-million-square-meter plant considered in this work. These factors may affect both separation efficiency and energy demand in real systems. Therefore, while the simulation results indicate the technological promise of the proposed cascade concept, further experimental validation is essential. Pilot-scale studies and intermediate-scale demonstrations are required to verify membrane performance under realistic wet flue gas conditions, assess scale-up effects, and confirm the practical feasibility of the proposed process configurations.

Author Contributions: Conceptualization, M.E.A. and A.N.P.; Methodology, K.A.S., V.V.Z. and S.S.S.; Validation, S.S.K.; Formal analysis, A.A.S. and A.V.V.; Investigation, M.E.A., V.V.Z. and A.N.P.; Data curation, K.A.S., S.S.K., A.A.S., S.S.S. and A.V.V.; Writing—original draft, A.A.A. and N.S.T.; Writing—review & editing, N.S.T.; Supervision, A.A.A. and I.V.V.; Project administration, I.V.V. All authors have read and agreed to the published version of the manuscript.

Funding: This work was carried out with the financial support of the Ministry of Science and Higher Education of the Russian Federation within the framework of scientific project No 075-15-2024-547.

Data Availability Statement: The original contributions presented in this study are included in the article. Further inquiries can be directed to the corresponding author.

Conflicts of Interest: The authors declare no conflict of interest.

References

1. Choudhry, T.; Kayani, U.N.; Gul, A.; Haider, S.A.; Ahmad, S. Carbon emissions, environmental distortions, and impact on growth. *Energy Econ.* **2023**, *126*, 107040. [CrossRef]
2. Chen, H.; Lu, J.; Obobisa, E.S. Striving towards 2050 net zero CO_2 emissions: How critical are clean energy and financial sectors? *Heliyon* **2023**, *9*, e22705. [CrossRef]
3. Looyd, P.J.D. Precombustion technologies to aid carbon capture. In *Greenhouse Gas Control Technologies*; Elsevier Science Ltd.: Amsterdam, The Netherlands, 2005; pp. 1957–1961. [CrossRef]
4. Ghoniem, A.F.; Zhao, Z.; Dimitrakopoulos, G. Gas oxy combustion and conversion technologies for low carbon energy: Fundamentals, modeling and reactors. *Proc. Combust. Inst.* **2019**, *37*, 33–56. [CrossRef]
5. Raganati, F.; Ammendola, P. CO_2 Post-combustion Capture: A Critical Review of Current Technologies and Future Directions. *Energy Fuels* **2024**, *38*, 13858–13905. [CrossRef]
6. Boer, D.G.; Langerak, J.; Pescarmona, P.P. Zeolites as Selective Adsorbents for CO_2 Separation. *ACS Appl. Energy Mater.* **2023**, *6*, 2634–2656. [CrossRef]
7. Raganati, F.; Miccio, F.; Ammendola, P. Adsorption of Carbon Dioxide for Post-combustion Capture: A Review. *Energy Fuels* **2021**, *35*, 12845–12868. [CrossRef]
8. Zanco, S.E.; Pérez-Calvo, J.-F.; Gasós, A.; Cordiano, B.; Becattini, V.; Mazzotti, M. Postcombustion CO_2 Capture: A Comparative Techno-Economic Assessment of Three Technologies Using a Solvent, an Adsorbent, and a Membrane. *ACS Eng. Au* **2021**, *1*, 50–72. [CrossRef]
9. Hack, J.; Maeda, N.; Meier, D.M. Review on CO_2 Capture Using Amine-Functionalized Materials. *ACS Omega* **2022**, *7*, 39520–39530. [CrossRef]

10. Laribi, S.; Dubois, L.; De Weireld, G.; Thomas, D. Study of the post-combustion CO_2 capture process by absorption-regeneration using amine solvents applied to cement plant flue gases with high CO_2 contents. *Int. J. Greenh. Gas Control* **2019**, *90*, 102799. [CrossRef]
11. Isogai, H.; Nakagaki, T. Mechanistic analysis of post-combustion CO_2 capture performance during amine degradation. *Int. J. Greenh. Gas Control* **2022**, *114*, 103597. [CrossRef]
12. Du, J.; Yang, W.; Xu, L.; Bei, L.; Lei, S.; Li, W.; Liu, H.; Wang, B.; Sun, L. Review on post-combustion CO_2 capture by amine blended solvents and aqueous ammonia. *Chem. Eng. J.* **2024**, *488*, 150954. [CrossRef]
13. Fu, L.; Ren, Z.; Si, W.; Ma, Q.; Huang, W.; Liao, K.; Huang, Z.; Wang, Y.; Li, J.; Xu, P. Research progress on CO_2 capture and utilization technology. *J. CO_2 Util.* **2022**, *66*, 102260. [CrossRef]
14. Kumar, H.; Sharma, R.; Malik, A.K.; Sharma, A.K.; Kumar, P.; Singh, D. Advancements in carbon capture and utilization technologies: Transforming CO_2 into valuable resources for a sustainable carbon economy. *Next Energy* **2026**, *10*, 100476. [CrossRef]
15. Zhao, T.; Li, R.; Zhang, Z.; Song, C. Current status of onboard carbon capture and storage (OCCS) system: A survey of technical assessment. *Carbon Capture Sci. Technol.* **2025**, *15*, 100402. [CrossRef]
16. Du, X.; Khan, M.N.; Thakur, G.C. Machine Learning in Carbon Capture, Utilization, Storage, and Transportation: A Review of Applications in Greenhouse Gas Emissions Reduction. *Processes* **2025**, *13*, 1160. [CrossRef]
17. Sun, Q.; Xiong, J.; Gao, H.; Olson, W.; Liang, Z. Energy-efficient regeneration of amine-based solvent with environmentally friendly ionic liquid catalysts for CO_2 capture. *Chem. Eng. Sci.* **2024**, *283*, 119380. [CrossRef]
18. He, X.; He, H.; Barzagli, F.; Amer, M.W.; Li, C.; Zhang, R. Analysis of the energy consumption in solvent regeneration processes using binary amine blends for CO_2 capture. *Energy* **2023**, *270*, 126903. [CrossRef]
19. Rochelle, G.T. Thermal degradation of amines for CO_2 capture. *Curr. Opin. Chem. Eng.* **2012**, *1*, 183–190. [CrossRef]
20. Bedell, S.A. Oxidative degradation mechanisms for amines in flue gas capture. *Energy Procedia* **2009**, *1*, 771–778. [CrossRef]
21. Voice, A.K.; Rochelle, G.T. Oxidation of amines at absorber conditions for CO_2 capture from flue gas. *Energy Procedia* **2011**, *4*, 171–178. [CrossRef]
22. Gao, J.; Wang, S.; Zhou, S.; Zhao, B.; Chen, C. Corrosion and degradation performance of novel absorbent for CO_2 capture in pilot-scale. *Energy Procedia* **2011**, *4*, 1534–1541. [CrossRef]
23. Park, J.W.; Heo, S.; Yeo, J.G.; Lee, S.; Kim, J.K.; Lee, J.H. Membrane-Based CO_2 Capture Across Industrial Sectors: Process Conditions, Case Studies, and Implementation Insights. *Membranes* **2025**, *15*, 200. [CrossRef]
24. Pazani, F.; Shariatifar, M.; Maleh, M.S.; Alebrahim, T.; Lin, H. Challenge and promise of mixed matrix hollow fiber composite membranes for CO_2 separations. *Sep. Purif. Technol.* **2023**, *308*, 122876. [CrossRef]
25. Favre, E. Carbon dioxide recovery from post-combustion processes: Can gas permeation membranes compete with absorption? *J. Memb. Sci.* **2007**, *294*, 50–59. [CrossRef]
26. Yang, D.; Wang, Z.; Wang, J.; Wang, S. Potential of Two-Stage Membrane System with Recycle Stream for CO_2 Capture from Postcombustion Gas. *Energy Fuels* **2009**, *23*, 4755–4762. [CrossRef]
27. Zhao, L.; Riensche, E.; Weber, M.; Stolten, D. Cascaded Membrane Processes for Post-Combustion CO_2 Capture. *Chem. Eng. Technol.* **2012**, *35*, 489–496. [CrossRef]
28. Micari, M.; Dakhchoune, M.; Agrawal, K.V. Techno-economic assessment of postcombustion carbon capture using high-performance nanoporous single-layer graphene membranes. *J. Memb. Sci.* **2021**, *624*, 119103. [CrossRef]
29. Tian, Z.; Mahurin, S.M.; Dai, S.; Jiang, D. Ion-Gated Gas Separation through Porous Graphene. *Nano Lett.* **2017**, *17*, 1802–1807. [CrossRef] [PubMed]
30. He, G.; Huang, S.; Villalobos, L.F.; Zhao, J.; Mensi, M.; Oveisi, E.; Rezaei, M.; Agrawal, K.V. High-permeance polymer-functionalized single-layer graphene membranes that surpass the postcombustion carbon capture target. *Energy Environ. Sci.* **2019**, *12*, 3305–3312. [CrossRef]
31. GitHub—CCSI-Toolset/membrane_model: Membrane Separation Model: Updated Hollow Fiber Membrane Model and System Example for Carbon Capture. Available online: https://github.com/CCSI-Toolset/membrane_model (accessed on 25 November 2021).
32. Merkel, T.C.; Lin, H.; Wei, X.; Baker, R. Power plant post-combustion carbon dioxide capture: An opportunity for membranes. *J. Memb. Sci.* **2010**, *359*, 126–139. [CrossRef]
33. Kniep, J.; Sun, Z.; Lin, H.; Mohammad, M.; Thomas-Droz, S.; Vu, J.; He, Z.; Merkel, T.; Amo, K. *Field Tests of MTR Membranes for Syngas Separations: Final Report of CO_2-Selective Membrane Field Test Activities at the National Carbon Capture Center*; Membrane Technology and Research, Inc.: Newark, CA, USA, 2017.
34. Hwang, S.-T.; Thorman, J.M. The continuous membrane column. *AIChE J.* **1980**, *26*, 558–566. [CrossRef]
35. Vorotyntsev, V.; Drozdov, P.N. Ultrapurification of gases in a continuous membrane column cascade. *Sep. Purif. Technol.* **2001**, *22–23*, 367–376. [CrossRef]

36. Huang, Y.; Merkel, T.C.; Baker, R.W. Pressure ratio and its impact on membrane gas separation processes. *J. Memb. Sci.* **2014**, *463*, 33–40. [CrossRef]
37. Robeson, L.M. The upper bound revisited. *J. Memb. Sci.* **2008**, *320*, 390–400. [CrossRef]
38. Zhang, Z.; Rao, S.; Han, Y.; Pang, R.; Ho, W.S.W. CO_2-selective membranes containing amino acid salts for CO_2/N_2 separation. *J. Memb. Sci.* **2021**, *638*, 119696. [CrossRef]
39. Comesaña-Gándara, B.; Chen, J.; Bezzu, C.G.; Carta, M.; Rose, I.; Ferrari, M.C.; Esposito, E.; Fuoco, A.; Jansen, J.C.; McKeown, N.B. Redefining the Robeson upper bounds for CO_2/CH_4 and CO_2/N_2 separations using a series of ultrapermeable benzotriptycene-based polymers of intrinsic microporosity. *Energy Environ. Sci.* **2019**, *12*, 2733–2740. [CrossRef]
40. Liu, M.; Nothling, M.D.; Zhang, S.; Fu, Q.; Qiao, G.G. Thin film composite membranes for postcombustion carbon capture: Polymers and beyond. *Prog. Polym. Sci.* **2022**, *126*, 101504. [CrossRef]
41. Batoon, V.; Borsaly, A.; Casillas, C.; Hofmann, T.; Huang, I.; Kniep, J.; Merkel, T.; Paulaha, C.; Salim, W.; Westling, E. Scale-Up Testing of Advanced PolarisTM Membrane CO_2 Capture Technology. *SSRN Electron. J.* **2022**, 23–24. [CrossRef]
42. Bozorg, M.; Ramírez-Santos, Á.A.; Addis, B.; Piccialli, V.; Castel, C.; Favre, E. Optimal process design of biogas upgrading membrane systems: Polymeric vs high performance inorganic membrane materials. *Chem. Eng. Sci.* **2020**, *225*, 115769. [CrossRef]

Disclaimer/Publisher's Note: The statements, opinions and data contained in all publications are solely those of the individual author(s) and contributor(s) and not of MDPI and/or the editor(s). MDPI and/or the editor(s) disclaim responsibility for any injury to people or property resulting from any ideas, methods, instructions or products referred to in the content.